# Dependent Thermo-Mechanical Behavior of Novel Alumina-Based Refractories

## A. Böhm[1], C.G. Aneziris[2] and J. Malzbender[*1]

[1]Institute of Energy and Climate Research - 2, Forschungszentrum Jülich GmbH,
Wilhelm-Johnen-Strasse, D-52425 Jülich, Germany
[2]Institute of Ceramic, Glass and Construction Materials, TU Bergakademie
Freiberg, Agricolastrasse 17, D-09596 Freiberg, Germany

## Abstract

Novel alumina-based refractories were assessed with regard to their thermo-mechanical behavior from room temperature to 1000 °C within the framework of the DFG SPP "FIRE" program. These refractories are being developed for use in slide gates or entry nozzles. Their elastic behavior was investigated with the impulse excitation technique. Wedge splitting tests were used to determine their fracture resistance behavior. The evaluated material characteristics and thermal shock resistance were compared to those of a standard refractory material, permitting conclusions to be drawn regarding the effect of the additives used (TiO$_2$, ZrO$_2$) on apparent elastic behavior, crack propagation and thermal shock resistance.

*Keywords: Refractories, ceramics, elastic modulus, fracture, thermal shock*

## I. Introduction

Their high corrosion resistance in contact with steel/slag has led to widespread use of alumina-based materials in refractory applications. Such refractories with high alumina content exhibit rather poor thermal shock resistance, which is usually enhanced with the addition of carbon [1]. However, this also increases the materials' thermal conductivity and hence energy consumption in industrial processes.

In the DFG Priority Program "FIRE", new refractory ceramics are being developed with the aim of reducing the necessary carbon content while preserving excellent thermal shock resistance. One of these is an alumina-based composite doped with TiO$_2$ and ZrO$_2$ (abbreviated AZT). The incorporation of small amounts of TiO$_2$ and ZrO$_2$ led to an improvement of the thermal shock behavior for these carbon-free materials [2]. In fact, it is suggested that the formation of new phases and the decomposition of Al$_2$TiO$_5$ lead to thermal expansion mismatches and thereby aid the formation of micro-crack networks [3, 4].

Since elastic modulus and fracture resistance are basic properties needed to assess failure and to determine thermal shock parameters [5], these parameters were studied at room and elevated temperatures up to 1000 °C and compared for AZT and pure alumina using impulse excitation and wedge splitting, respectively. In order to explain the observed rather complex behavior, complementary elevated-temperature X-ray diffraction (XRD) investigations were also performed.

## II. Experimental

The investigated materials were produced at the TU Freiberg. One is a pure alumina (A1) and the second a 95-wt.% alumina doped with 2.5 wt.% of both TiO$_2$ and ZrO$_2$ (A1AZT). All materials were sintered at 1600 °C for 2 hours. The open porosity is 12.7 and 13.9 % for A1 and A1AZT, respectively [6]. The maximum grain size is 1 mm for both materials with similar grain size distributions. A detailed description of the production and microstructural images can be found in [7]. The composition of the raw materials is listed in Table 1. Aneziris *et al.* [4] investigated the microstructure of a fine-grained AZT-material. They derived a thermal expansion coefficient model based on the different expansion coefficients of Al$_2$O$_3$-, ZrO$_2$- and TiO$_2$-rich zones. The model suggests that a micro-crack network forms during thermal cycling owing to the large mismatches of the thermal expansion behavior of the different zones dominated by the different oxides.

An impulse excitation technique was used to assess the elastic behavior. Based on the resonant frequency of the fundamental bending mode ($f_f$), the apparent elastic modulus of bar-shaped specimens can be calculated following ASTM E 1876 − 01 [8]:

$$E = 0.9465 \cdot \left( \frac{m \cdot f_f^2}{b} \right) \left( \frac{L^3}{t^3} \right) T_1 \qquad (1)$$

* Corresponding author: j.malzbender@fz-juelich.de

**Table 1:** Composition of A1 and A1AZT

| Raw materials/Producer | Particle size [mm] | Composition [wt%] | |
|---|---|---|---|
| | | A1 | A1AZT |
| Alumina, T60 – 64/Almatis | 1.0 – 0.5 | 13 | 12.35 |
| | 0.6 – 0.2 | 10 | 9.50 |
| | 0.5 – 0 | 10 | 9.50 |
| | 0.2 – 0 | 25 | 23.75 |
| | 0.045 – 0 | 12 | 11.40 |
| | 0.020 – 0 | 10 | 9.50 |
| Alumina, CT9FG/Almatis | 0.007 – 0.002 | | |
| Alumina, Martoxid/Martinswerk | 0.0008 | 20 | 19 |
| 3.5 wt% Mg-PSZ/Saint Gobain | $d_{50} = 1.1\ \mu m$ | | 2.50 |
| Titania, Tronox T-R/Crenox | $d_{50} = 1.0\ \mu m$ | | 2.50 |

where $m$ is mass, $L$ length, $b$ width, $t$ height and $T_1$ a geometry correction factor. Measurements were conducted using a commercial GrindoSonic set-up (Lemmens N.V., Belgium) from room temperature (RT) to 1000 °C. A bar geometry of $45 \times 14 \times 6$ mm³ was chosen, taking into account the limited space of the test set-up, while still ensuring the required height/maximum grain size and length/height ratio of $> 5$ [7]. Complementary powder XRD was used to analyze the phase composition. The measurements were performed using a D5000 X-ray diffractometer (Siemens, Germany) from RT to 1000 °C.
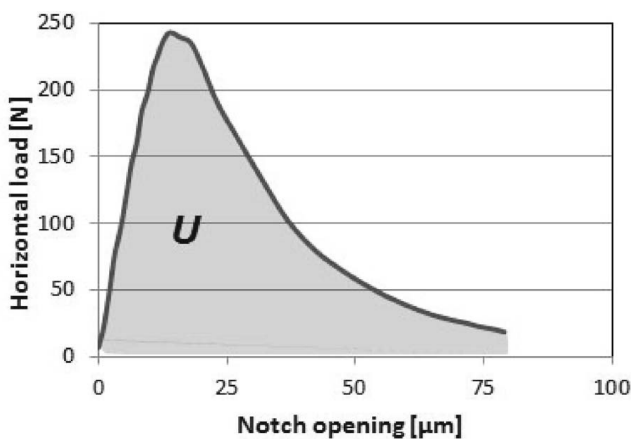


**Fig. 1a:** Load-notch opening curve from a WST.

Wedge splitting tests (WST) were conducted to determine the crack resistance $R$ and thermal shock parameter $R''''$. The WST is a commonly used method to determine the work of fracture (WOF) for brittle materials. With this method, pre-notched samples of cubic or rectangular shape (cylindrical samples are also possible) are loaded by means of a wedge that is driven into the notch with a constant displacement speed. When stable crack propagation is reached for the whole splitting process, WOF (and therefore $R''''$ values) and also $R$-curves can be calculated from the horizontal load-displacement diagrams (Fig. 1a; see also below for a more detailed explanation). The experimental set-up is based on the method reported by Tsechegg [9, 10] and was modified since small samples

were necessary for tests with *in-situ* observation in SEM, which have been reported previously [6]. Further information on the microstructure and porosity as well as information on impurities and micro-cracks can also be found in this work.

The reduction of the specimen size permitted a higher number of tests since efforts for specimen preparation and experiment duration were reduced. The horizontal displacement at RT was measured using displacement transducers. To assess specimen geometry effects in the current study, samples of $20 \times 20 \times 20$ mm³ and $40 \times 40 \times 20$ mm³ were tested. High-temperature (HT, up to 1000 °C) experiments were performed in an Instron testing machine. A long-distance microscope was used since the notch opening at HT could not be measured directly, recording 30 images per minute (resolution 1.7 μm/pixel). The notch opening was determined from these images, which were synchronized with the vertical force data. All experiments were conducted using a vertically crosshead speed of 25 μm/min. Either a metallic (RT, angle $a$ of 40°) or a ceramic wedge (HT, $a$ of 20°) was used. The horizontal force ($F_H$) was calculated from the applied vertical force ($F_V$) with:

$$F_H = \mu \cdot \frac{F_V}{2\tan\left(\frac{\alpha}{2}\right)} \qquad (2)$$

For the friction coefficient $\mu$, a value of 0.24 was used [6]. Fig. 1b illustrates schematically a WST set-up. Seven small A1 and seven small A1AZT samples were tested at RT. Additionally one A1 and one A1AZT with the geometry $40 \times 40 \times 20$ mm³ were tested and one $20 \times 20 \times 20$ mm³ sample at HT.

The crack resistance $R$ was determined in order to gain insight into the crack propagation behavior. It was calculated from the load-displacement curves by applying the energy based concept after Bornhauser *et al.* [11]. The crack length was calculated using a compliance function derived by Saxena and Hudak [12]. The notch opening-vertical displacement behavior was described by mathematical fits in order to limit the effect of uncertainties of individual data points in the HT load-notch opening curves. For the

increasing (elastic) part of the load displacement curve, a linear fit was chosen. The decreasing (notch opening) part could be described well with a logarithmic equation of the form $(a + b \cdot \ln(x + c))$ (see Fig. 2a). The calculated load-notch opening curve is shown in Fig. 2b.



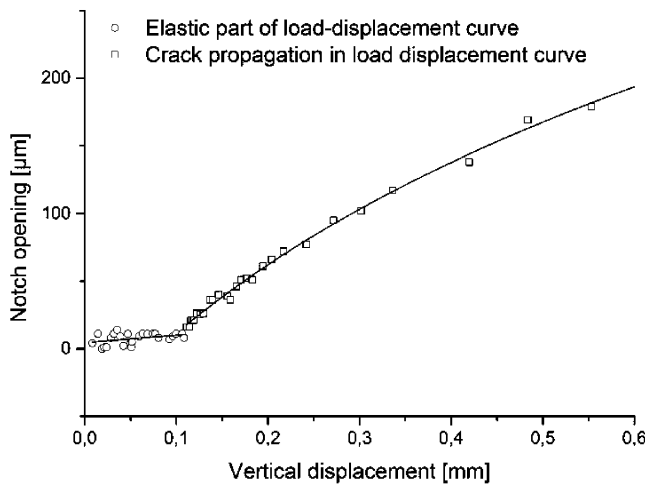**Fig. 1b:** Experimental set-up for WST at RT.
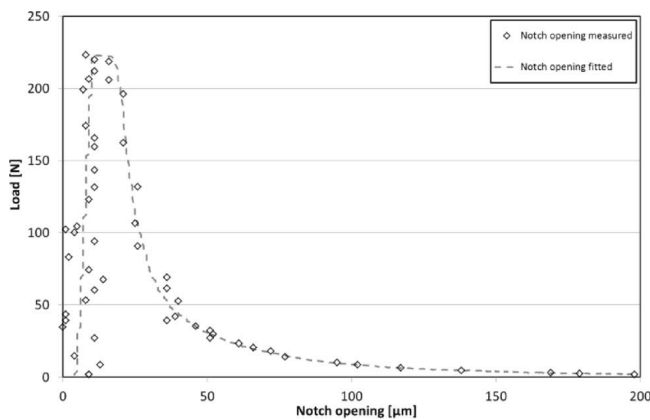


**Fig. 2a:** HT WST fit of notch opening.



**Fig. 2b:** HT WST load-notch opening curve.

The area under the curve in Fig. 1a is the dissipated energy $U$. The work of fracture ($\gamma_{WOF}$) can be calculated via its ratio in respect of the fracture surface areas ($2A$):

$$\gamma_{WOF} = \frac{1}{2A} \int_0^{\delta_{H,max}} F_H d\delta_H \qquad (3)$$

RT elastic modulus $E$ and fracture strength $\sigma_f$ data were provided by TU Freiberg (Table 2) based on ultrasonic run-time and three-point bending tests, respectively, permitting finally a calculation of the thermal shock parameter $R''''$:

$$R'''' = \frac{\gamma_{WOF} \cdot E}{\sigma_f^2} \qquad (4)$$

**Table 2:** Elastic moduli and fracture strengths used for the calculation of $R''''$

|  | A1 | A1AZT |
|---|---|---|
| Elastic modulus/GPa | $166 \pm 2$ | $68 \pm 12$ |
| Fracture strength/MPa | $88 \pm 8$ | $15 \pm 1$ |

## III. Results and Discussion

The temperature dependences of the apparent elastic moduli A1 and A1AZT are compared in Fig. 3. The modulus of A1 decreases linearly by ~ 11 % with increasing temperature from RT to 1000 °C (see Fig. 3a), which agrees with the typical behavior of ceramic materials [13]. For the material A1, congruent curves were obtained for heating and cooling. Contrary to this, A1AZT reveals in the first heating cycle a strong modulus decrease of about 60 % up to ~ 500 °C, which was not observed anymore in reheating experiments (see Fig. 3b). Repeated heating cycles were carried out for the AZT materials and more curves and details are given in [6]. In fact, this decrease was not observed in four-point bending experiments, suggesting that the effect might be a result of sample preparation. Decreases of the modulus in a similar temperature range have been associated in the past with dehydration effects or decomposition of binders [14]. Initial investigations suggest that the glue used for sample preparation affected the measured elastic properties for the current material remnants. This glue decomposes completely at 550 °C.
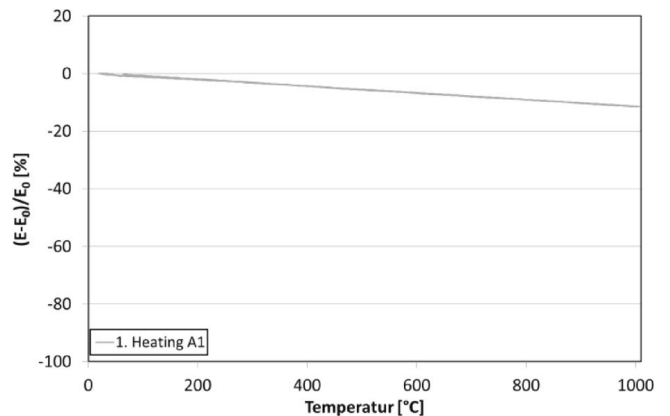


**Fig. 3a:** Relative change of elastic modulus with temperature of A1.

At higher temperatures a strong hysteresis effect is observed (that also occurred in reheating experiments), the modulus increase starts at about 800 °C during heating and the decrease during cooling starts at about 650 °C. XRD investigations verified that this effect corresponds to the occurrence of a $ZrO_2$ phase transition (see Fig. 4). The purely monoclinic $ZrO_2$ phase that exists at low temper-

ature completely transforms to a tetragonal phase at about 900 °C, which transforms back to the monoclinic phase during cooling down below 500 °C. It might be expected that such a phase transition would occur above 1000 °C, but the incorporation of $TiO_2$ in the $ZrO_2$ lattice lowers the transition temperature [15]. Although no microstructural changes could be observed after the heating cycles, the phase transition is accompanied by a volume change of 3 to 5 %, which might lead to debonding and damage, similar to that reported for other refractory composites where modulus effects were related to damage owing to thermal expansion mismatch between grains and matrix [16]. Sintering effects owing to exposure to the testing temperature are not observed and are also not expected since the preparation of the materials involves a sintering step at 1600 °C.
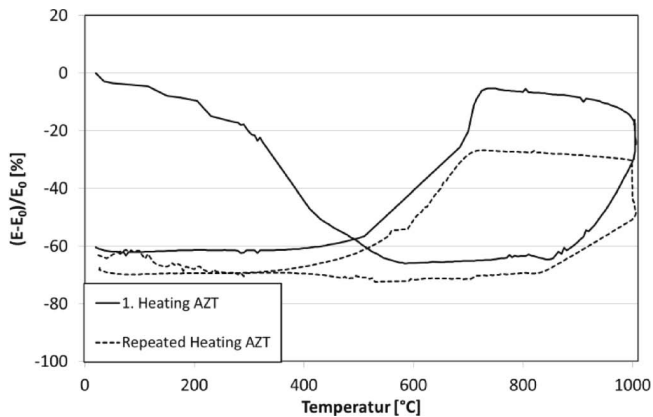


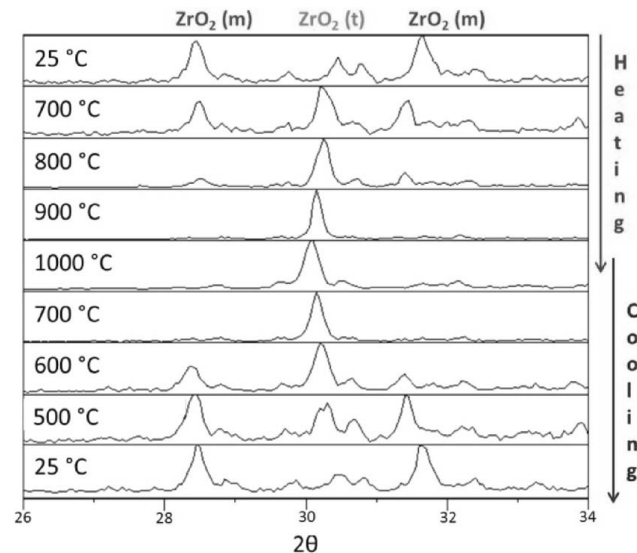**Fig. 3b:** Relative change of elastic modulus with temperature of A1AZT.



**Fig. 4:** Excerpt of the XRD pattern of A1AZT.

For refractory ceramics it is preferred to have a rising *R*-curve behavior, implying low crack initiation energies but limited crack extension that avoids catastrophic failure. Pure alumina shows at RT a linear proportionality of crack resistance and crack length (see Fig. 5). In fact, the crack resistance of alumina has already been reported in various studies [17, 18]. It has been verified in [19] that the main mechanism for a rising *R*-curve is a "wake zone shielding" owing to specific microstructure-related physical contacts between rough fracture surfaces (large grains

in a matrix). It can be expected that crack resistance reaches a plateau value once the crack opening is large enough such that the length of the contact zone remains constant. Although previous investigations using a compact tension set-up confirmed this plateau for A1 [6], neither the small nor the bigger sample used in the current study seem to be sufficient to reach this plateau value, implying that there is no equilibrium in fracture surface interaction even for the sample with a length of 40 mm (see Fig. 5).
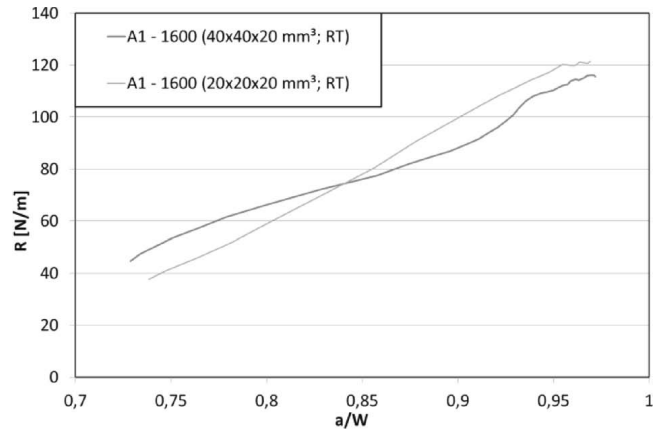


**Fig. 5:** Fracture resistance as a function of normalized crack depth for A1 – 1600.

The RT *R*-curve of AZT (see Fig. 6) reveals a similar behavior as A1 at HT. The crack initiation energy is lower than for A1 at RT but reaches higher values when the normalized crack extends to $a/W > 0.9$. It has been verified in previous works [6] using *in-situ* SEM wedge splitting experiments that crack branching is the main shielding mechanism for AZT.
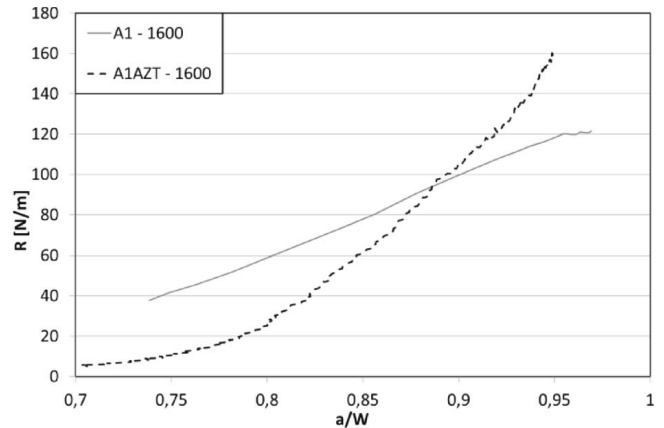


**Fig. 6:** Fracture resistance as a function of normalized crack depth for A1 – 1600 and A1AZT - 1600.

The alumina *R*-curve behavior was also studied at 1000 °C in order to investigate crack propagation closer to service conditions. The elastic modulus used for calculation of the crack length was estimated to be 150 GPa (assuming a decrease of ~ 1 % per 100 °C). *R*-curves obtained experimentally along with the fitted notch openings are shown in Fig. 7. The shape of the HT *R*-curve differs from the one obtained at RT, which might be an indication of a different crack propagation mechanism related to a larger elevated-temperature ductility. However, the HT experimental procedure still needs further refinement since the

notch opening cannot be measured as accurately as at RT and the friction correction is based on RT experiments. The notch opening values obtained from the mathematical description might not be valid for the crack initiation and/or low $a/W$, thus the beginning of the $R$-curve might be inaccurate. Furthermore, for the HT measurements a wedge with an angle of 20° was used, whereas a 40° wedge was used at RT (the use of different wedge angles resulted in different horizontal displacement speeds).
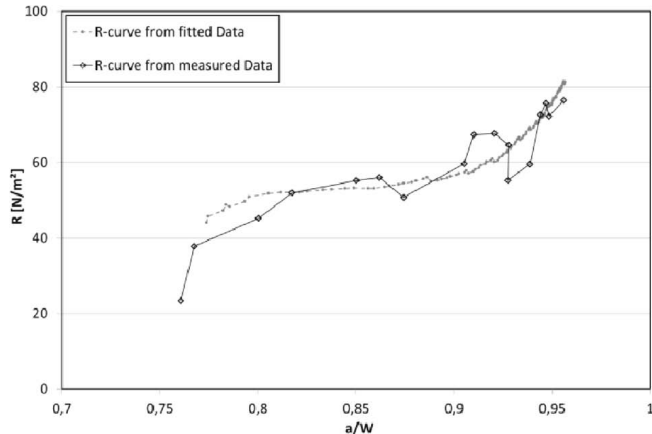


**Fig. 7:** Fracture resistance as a function of normalized crack depth for A1 – 1600 at 1000 °C.

Finally, Table 3 summarizes the results for work of fracture and $R''''$. A high $R''''$ value implies a higher damage resistance and therefore indicates better thermal shock resistance. No difference is observed for different sample geometries in the case of pure alumina, for samples with the same relative notch depth. Previous results have shown that the work of fracture decreases with increasing notch depth for small AZT samples (20 × 20 × 20 mm³) in [6]. Thus a size effect is not negligible for the small samples. The specimen geometry was not varied for AZT. At 1000 °C the alumina work of fracture is lower than at RT ($R''''$ was not calculated since $\sigma_f$ data were not available at the time). A1AZT yields lower work of fracture values and a higher $R''''$, which indicates improved thermal shock behavior.

**Table 3:** Work of fracture and $R''''$ (size * 20 × 20 × 20 mm³ and ** 40 × 40 × 20 mm³)

| | A1 (RT)* | A1 (RT)** | A1 (1000 °C)* | A1AZT (RT)* |
|---|---|---|---|---|
| WOF (N/m) | 38 ± 4 | 36 | 21 | 27 ± 3 |
| $R''''$ (mm) | 0.8 ± 0.1 | 0.8 | - | 8 ± 1 |

## IV. Conclusions

Thermo-mechanical properties of refractory materials were measured at RT and elevated temperatures. Addition of small amounts of $ZrO_2$ and $TiO_2$ led to large changes in elastic modulus and thermal shock resistance. The apparent dynamic elastic modulus for alumina decreased linearly with increasing temperature. The AZT materials exhibited a complex temperature-dependent elastic modulus behavior partly occurring along with an experimentally confirmed $ZrO_2$ phase transition, which might also affect the thermal shock behavior.

The additives also led to different $R$-curve behavior compared to pure alumina. The $R$-curves showed different behavior at 1000 °C than at RT for pure alumina, which might be related to the materials' higher ductility. AZT refractories are predicted to have an improved thermal shock resistance compared to alumina based on RT data owing to a different crack growth mechanism.

Experiments at higher temperatures are planned since application temperatures for sliding gates and entry nozzles are significantly higher than the current test temperature, which requires an improvement of the horizontal displacement measurement accuracy. A determination of $R''''$ parameters based on elevated-temperature fracture stresses will be the focus of further work.

## Acknowledgement

## References

[1] Li, Y.W., Aneziris, C.G., Yi, X.X., Jin, S.L., Li, N.: Formation of dumbbell-shaped β-SiC for the manufacturing of advanced composite refractories in the system $Al_2O_3$-$ZrO_2$-C, *Interceram-Refractory Manual*, 20 – 23, (2005).

[2] Aneziris, C.G., Dudczig, S., Gerlach, N., Berek, H., Veres, D.: Thermal shock performance of fine-grained $Al_2O_3$ ceramics with $TiO_2$ and $ZrO_2$ additions for refractory applications, *Adv. Eng. Mater.,* **12**, [6], 478 – 485, (2010).

[3] Ohya, Y., Nakagawa, Z.: Grain-boundary microcracking due to thermal expansion anisotropy in aluminum titanate ceramics, *J. Am. Ceram. Soc.*, **70**, [8], 184 – 186, (1987).

[4] Aneziris, C.G., Schaerfl, W., Ullrich, B.: Microstructure evaluation of $Al_2O_3$ ceramics with Mg-PSZ- and $TiO_2$-additions, *J. Eur. Ceram. Soc.*, **27**, [10], 3191 – 3199, (2007).

[5] Hasselman, D.P.H.: Thermal stress resistance parameters for brittle refractory ceramics – a compendium, *Am. Ceram. Soc. Bull.*, **49**, [12], 1033 – 1037, (1970).

[6] Skiera, E.: Thermomechanical characterization of newly developed refractories, (in German), Ph.D. Thesis, RWTH Aachen, (2012).

[7] Skiera, E., Malzbender, J., Mönch, J., Dudczig, S., Aneziris C.G., Steinbrech, R.W.: Controlled crack propagation experiments with a novel alumina-based refractory, *Adv. Eng. Mater.*, **14**, [4], 248 – 254, (2012).

[8] ASTM E 1876 – 01: Standard test method for dynamic young's modulus, shear modulus, and poisson's ratio by impulse excitation of vibration, (2005).

[9] Tschegg, E.: Test set-up for determining characteristic fracture-mechanical values and appropriate test specimens, (in German), AT 390 328 B, (1986).

[10] Tschegg, E.: Set-up for introducing loads, (in German), AT 396 997 B, (1994).

[11] Bornhauser, A., Kromp, K., Pabst, R.F.: R-curve evaluation with ceramic materials at elevated temperatures by an energy approach using direct observation and compliance calculation of the crack length, *J. Mater. Sci.*, **20**, 2585 – 2596, (1985).

[12] Saxena, A. Hudak, S.J.: Review and extension of compliance information for common crack growth specimens, *Int. J. Fracture*, **14**, [5], 453 – 468, (1978).

[13] Wachtman jr., J.B., Tempt, W.E., Lam Jr., D.G., Apstkin, C.S.: Exponential temperature dependence of Young's modulus for several oxides, *Phy. Rev.*, **122**, [6], 1754 – 1759, (1961).

14 Souza, T.M., Mati, A.P.M., Brito, M.A.M., Pandolfelli, V.C.: Oxidation protection system for hot elastic modulus evaluation of refractory ceramics, *Ceram. Int.*, (in press).

15 Pandolfelli, V.C., Rodriguez, J.A., Stevens, R.: Effects of $TiO_2$ addition on the sintering of $ZrO_2 \cdot TiO_2$ compositions and on the retention of the tetragonal phase of zirconia at room temperature, *J. Mater. Sci.*, **26**, 5327 – 5334, (1991).

16 Joliff, Y., Absi, J., Huger, M., Glandus, J.C.: Experimental and numerical study of the elastic modulus vs. temperature of debonded model materials, *Comp. Mater. Sci.*, **44**, [2], 826 – 831, (2008).

17 Hübner, H., Jillek, W.: Subcritical crack extension and crack resistance in polycrystalline alumina, *J. Mater. Sci.*, **12**, 117 – 125, (1977).

18 Sakai, M., Bradt, R.C.: The crack growth resistance of non-phase-transforming ceramics, *J. Ceram. Soc. Jpn.*, **96**, [8], 801 – 809, (1988).

19 Steinbrech, R.W., Reichl, A., Schaarwachter, W.: R-curve behavior of long cracks in alumina, *J. Am. Ceram. Soc.*, **73**, [7], 2009 – 2015 (1990).